Gold and Hairpin DNA Functionalization of Upconversion Nanocrystals for Imaging and In Vivo Drug Delivery

Sanyang Han, Animesh Samanta, Xiaoji Xie, Ling Huang, Juanjuan Peng, Sung Jin Park, Daniel Boon Loong Teh, Yongdoo Choi, Young-Tae Chang, Angelo Homayoun All,* Yanmei Yang, Bengang Xing, and Xiaogang Liu**

Although multifunctional upconversion imaging probes have recently attracted considerable interest in biomedical research, there are currently few methods for stabilizing these luminescent nanoprobes with oligonucleotides in biological systems. Herein, a method to robustly disperse upconversion nanoprobes in physiological buffers based on rational design and synthesis of nanoconjugates comprising hairpin-DNA-modified gold nanoparticles is presented. This approach imparts the upconversion nanoprobes with excellent biocompatibility and circumvents the problem of particle agglomeration. By combining single-band anti-Stokes near-infrared emission and the photothermal effect mediated by the coupling of gold to upconversion nanoparticles, a simple, versatile nanoparticulate system for simultaneous deep-tissue imaging and drug molecule release in vivo is demonstrated.

Luminescent biomarkers have drawn immense attention in the past decade because of their potential applications in biological labeling,[1] sensing,[2] molecular diagnostics,[3] and clinical therapeutics.[4] In particular, considerable efforts have been devoted to the development of near-infrared (NIR) to NIR luminescent probes.[5] Among them, lanthanide-doped upconversion nanoparticles, which are able to convert NIR excitation into shorter-wavelength emissions, show great promise for biolabeling due to their unique features such as high photochemical stability, sharp emission bandwidth, and large anti-Stokes shift.[6] Recently, upconversion nanoparticles have been widely used as luminescent biomarkers for bioapplications.[7] Despite the advances, the knowledge of surface functionalization for improved stability of upconversion nanoparticles in biological systems is far from being complete.

To render nanomaterials with a molecular functionality and high stability in biological settings, the crucial step is to develop a robust synthetic approach for surface modification with a high-density coverage of hydrophilic, biocompatible molecules. To meet this requirement, many strategies have been developed for functionalizing upconversion nanoparticles, including surface modification with polymers,[8] biomolecules,[9] or proteins.[10] Nevertheless, most of these strategies often suffer from complex synthetic processes and yield nanoparticles with limited biocompatibility, functionality, and dispersibility in high-salt

Dr. S. Han, Prof. A. H. All
Department of Orthopedic Surgery
National University of Singapore
Singapore 119228, Singapore
E-mail: angelo.all@nuhs.edu.sg
Dr. S. Han, Prof. X. Liu
Department of Chemistry
National University of Singapore
Singapore 117543, Singapore
E-mail: chmlx@nus.edu.sg
Dr. A. Samanta, Dr. J. Peng, Dr. S. J. Park, Prof. Y.-T. Chang
Singapore Bioimaging Consortium
Agency for Science
Technology and Research (A*STAR)
Singapore 138667, Singapore
Dr. X. Xie, Prof. L. Huang
Key Laboratory of Flexible Electronics & Institute of Advanced Materials
Jiangsu National Synergetic Innovation Center for Advanced Materials
Nanjing Tech University
Nanjing 211816, P. R. China
E-mail: iamlhuang@njtech.edu.cn
Dr. D. B. L. Teh, Prof. A. H. All
Singapore Institute of Neurotechnology (SINAPSE)
Singapore 117456, Singapore
Prof. Y. Choi
Molecular Imaging & Therapy Branch
National Cancer Center
Gyeonggi-do 10408, Republic of Korea
Prof. A. H. All
Department of Biomedical Engineering
Johns Hopkins University School of Medicine
Baltimore, MD 21205, USA
Dr. Y. Yang, Prof. B. Xing
Division of Chemistry and Biological Chemistry
Nanyang Technological University
Singapore 637371, Singapore
Prof. X. Liu
SZU-NUS Collaborative Innovation Center for Optoelectronic Science & Technology
Key Laboratory of Optoelectronic Devices and Systems of Ministry of Education and Guangdong Province
Shenzhen University
Shenzhen 518060, P. R. China

DOI: 10.1002/adma.201700244

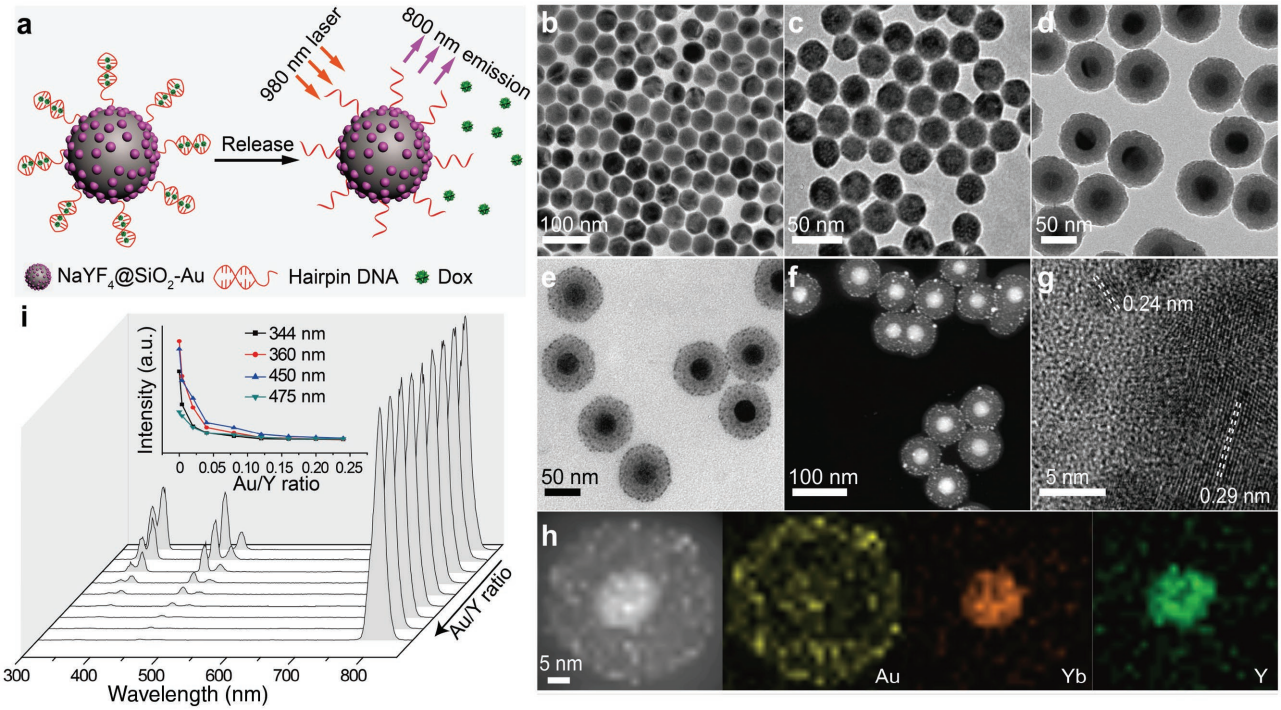

Figure 1. Design of hairpin DNA-functionalized $NaYF_4$@SiO_2–Au nanoparticles for photothermal drug release. a) Schematic illustration of Dox drug release from hpDNA-modified $NaYF_4$@SiO_2–Au nanoconjugates, triggered by a photon upconversion process. b–e) TEM images of the as-synthesized hydrophobic $NaYF_4$, ligand-free $NaYF_4$, $NaYF_4$@SiO_2, and $NaYF_4$@SiO_2–Au nanoparticles, respectively. f,g) The corresponding STEM and high-resolution TEM images of the $NaYF_4$@SiO_2–Au nanoparticles. h) Elemental mapping of a single $NaYF_4$@SiO_2–Au nanoparticle, indicating the spatial distribution of the Au, Yb, and Y elements in the core–shell structure. i) Photoluminescence response of a series of $NaYF_4$@SiO_2–Au nanoparticles, prepared with different Au/Y molar ratios (from back to front: 0, 0.004, 0.02, 0.04, 0.08, 0.12, 0.16, 0.20, 0.24). The inset shows the plot of luminescence intensity at 344, 360, 450, and 475 nm against the Au/Y molar ratio. The spectra were recorded at room temperature under excitation of a 980 nm CW diode laser with a power density of 4.6 W cm^{-1}.

physiological environment. Alternatively, DNA surface functionalization may offer a solution to solve these problems. For example, the surface modification of gold (Au) nanoparticles with DNA strands is known to significantly improve the particles' stability at high-salt buffer conditions.[11] In addition, the programmability inherent to DNA in terms of easy modulation in sequence and length can be exploited to impart the nanoparticles with a variety of functionalities.[12] However, a strong affinity between negatively charged phosphates of the DNA backbone and lanthanide ions can result in a random coordination of nucleotide bases to the particle's surface.[13] This is problematic as it can induce particle aggregation in aqueous solutions, especially at high-salt buffer conditions. Furthermore, the nonspecific binding between DNA backbones and lanthanides can prevent the ability of the DNA to hybridize to a target, which hampers intrinsic DNA functions for sensing, targeting, and gene expression.[14] Indeed, it has been challenging to stabilize DNA-modified upconversion nanoparticles in physiological buffers, while retaining biological function.

Herein, we report a design principle for stabilizing upconversion nanoparticles based on the coupling of small-sized Au nanoparticles (≈2 nm) and hairpin DNA (hpDNA) conjugation. In our proposal, a silica-shell coating on the surface of upconversion nanoparticles is also employed to block the direct interaction between the hpDNA strands and the nanoparticles. The hpDNA strands are immobilized onto Au nanoparticles using the well-known Au–thiol chemistry. The coupling of Au to upconversion nanoparticles allows us to modulate luminescence in the NIR region (≈800 nm) for minimal attenuation in tissues (**Figure 1**a). Moreover, the hpDNA strand allows a high drug loading capacity while maintaining temperature-sensing capability for fully controlled drug delivery. Together, these attributes make upconversion-Au nanoconjugates an ideal platform to achieve simultaneous deep-tissue imaging and site-specific administration of anticancer drugs (Figure 1a).

As a proof-of-concept experiment, we chose $NaYF_4$ as the host material due to its well documented high upconversion luminescence efficiency. We synthesized the $NaYF_4$ nanoparticles codoped with Yb^{3+} and Tm^{3+} by a coprecipitation process (Figure 1b and Figure S1 (Supporting Information)).[15] Subsequently, an acid treatment was conducted to remove the oleate ligands capped on the particle's surface (Figure 1c and Figure S2 (Supporting Information)). We then coated $NaYF_4$:Yb/Tm nanoparticles with a thin layer of silica shell by a modified literature procedure,[16] followed by amination functionalization of the silica shell (Figure 1d). With the availability of pendant amine functional groups, Au nanoparticles (≈2 nm) could be effectively attached to the silica surface. This was confirmed by transmission electron microscopy (TEM) and scanning TEM (STEM) imaging (Figure 1e,f). High-resolution TEM imaging of a single $NaYF_4$@SiO_2–Au nanoparticle shown in Figure 1g reveals lattice fringes of the (110) with a *d*-spacing

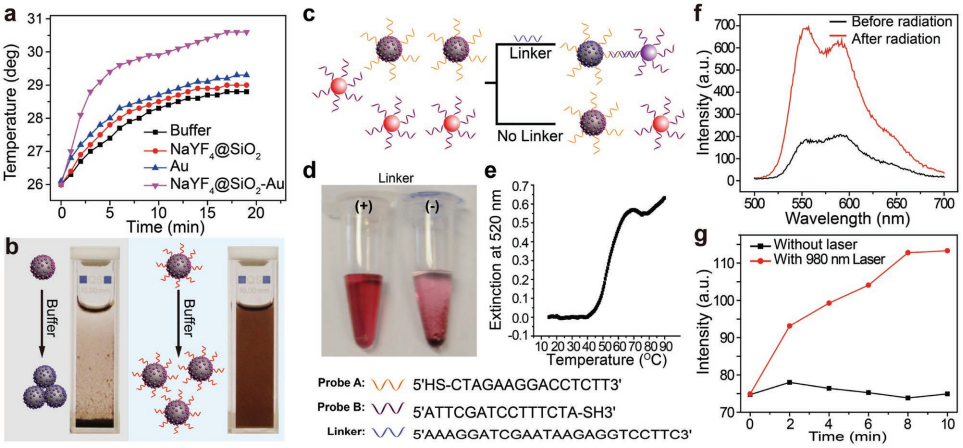

Figure 2. Photothermal effect and stability investigation of the as-prepared nanoconjugates. a) Time-dependent temperature profiles of $NaYF_4$@SiO_2–Au, $NaYF_4$@SiO_2, Au, and buffer solution (0.2 M NaCl, 10×10^{-3} M Tris-HCl), measured under the irradiation of a 980 nm laser at 500 mW cm^{-2}. b) Photographs showing colloidal stability of hpDNA-modified (right) and unmodified (left) $NaYF_4$@SiO_2–Au nanoconjugates in a buffer solution (0.2 M NaCl, 10×10^{-3} M Tris-HCl). c) Schematic design showing the formation of three-component sandwich structure using DNA-modified gold and $NaYF_4$@SiO_2–Au nanoparticles. d) Colorimetric responses of the reaction mixture containing DNA-modified gold and $NaYF_4$@SiO_2–Au nanoparticles in the absence and presence of linker DNA, respectively. e) The melting curves determined for the reaction mixture in the presence of linker DNA. f) Photoluminescence spectra of the solution containing Dox-loaded nanoconjugates before and after irradiation with a 980 nm laser (5 W cm^{-1}). g) Time-dependent photoluminescence studies showing the release of Dox molecules in the solution when illuminated with a 980 nm laser (5 W cm^{-1}).

of 0.29 nm and lattice fringes of the (111) with a *d*-spacing of 0.24 nm, attributable to hexagonal $NaYF_4$ and face-centered cubic Au, respectively. Energy-dispersive X-ray mapping analysis further confirmed the core–shell nature of the nanoconjugate (Figure 1h).

Next, we examined the photoluminescence properties of the $NaYF_4$:Yb/Tm@SiO_2–Au core–shell nanoparticles as a function of Au content. As shown in Figure 1i, the emission intensity of these core–shell nanoparticles in the ultraviolet–visible (UV–vis) range displayed a descending trend with increasing amounts of Au, while the emission at 800 nm is virtually unaltered (Figures S3–S5, Supporting Information). Notably, when the molar ratio of Au to Y exceeds 0.24, only the NIR emission peak could be observed. The selective quenching of upconversion emission in the UV–vis region by Au nanoparticles was ascribed to destructive interference between the excited state wavefunction of upconversion nanoparticles and the d–sp interband transition of Au nanoparticles. This quenching behavior requires the spectral overlap between the emission of the luminophore and the interband transition of Au nanocrystals.[17] Indeed, the UV–vis spectroscopic analysis revealed that there is a large overlap between the absorption spectrum of the Au nanoparticles and the emission spectrum of the upconversion nanoparticles in the UV–vis region (Figure S6, Supporting Information).

It is likely that the quenching of upconversion emission in the UV–vis region leads to an increase in the surface temperature of Au nanoparticles by the localized photothermal effect whereby the light absorbed by the Au nanoparticle is released as heat. The photothermal effect under NIR irradiation was confirmed by control experiments. As shown in **Figure 2**a, it was found that under identical experimental conditions, the temperature of a $NaYF_4$@SiO_2–Au suspension rises much faster than that of a solution containing either Au or $NaYF_4$@SiO_2 nanoparticles alone (Figure S7, Supporting Information).

The success of drug delivery in vivo depends largely upon the stability of the nanoconjugates under physiological conditions. For this purpose, we employed thiol-modified hpDNA to functionalize the surface of the as-prepared $NaYF_4$@SiO_2–Au nanoparticles because short synthetic DNA sequences are known to stabilize Au colloids over a wide range of buffer conditions. To demonstrate the feasibility of our approach, we ran two parallel sets of analysis to examine the stability of $NaYF_4$@SiO_2–Au and hpDNA-modified nanoconjugates suspended in a buffer solution (0.2 M NaCl, 10×10^{-3} M Tris-HCl). As anticipated, unmodified $NaYF_4$@SiO_2–Au nanoconjugates precipitated out of the solution after several minutes (Figure 2b). On the contrary, hpDNA-modified $NaYF_4$@SiO_2–Au counterparts remained dispersive even after storage for several months. In addition, our hpDNA-modified nanoconjugates also showed a good stability in other biofluids including Dulbecco's modified Eagle's medium and fetal bovine serum (Figure S8, Supporting Information). In a further set of experiments, the hpDNA modification was verified by agarose gel electrophoresis. Under an electric field, hpDNA-modified $NaYF_4$@SiO_2–Au nanoconjugates migrate faster through the agarose gel than their unmodified equivalents, suggesting the presence of charged DNA molecules on the surface of the nanoconjugates (Figure S9, Supporting Information). An intriguing aspect of using hpDNA is its high thermal sensitivity and ability to encapsulate small drug molecules into the double-helical framework. Thus, remote-controlled release of drug molecules can be realized with an NIR laser by means of the photothermal effect. To confirm whether the DNA strands tethered on the surface of $NaYF_4$@SiO_2–Au nanoparticles retain their biological functions, we tested their ability to specifically hybridize to complimentary DNA targets by reacting with another set of DNA-modified Au nanoparticles of ≈14 nm in diameter (Figure 2c–e). In the presence of a linker DNA strand, formation of particulate aggregates could be clearly visualized. In contrast, we did

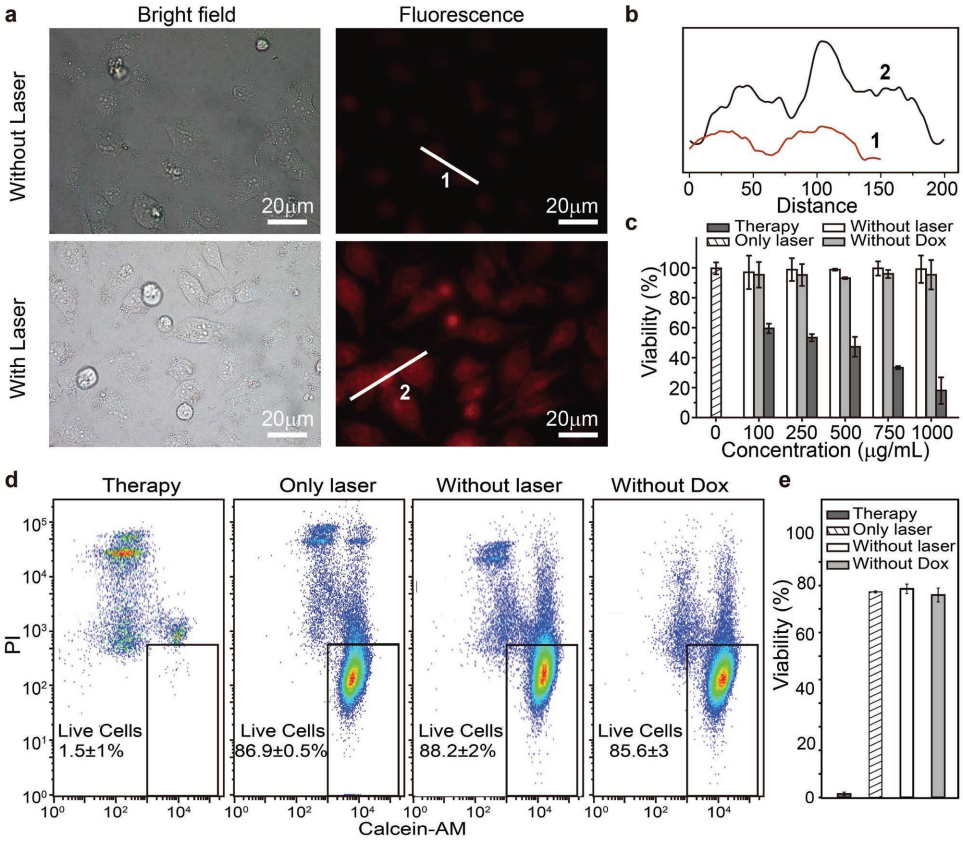

Figure 3. Intracellular uptake, imaging, and in vitro drug delivery of as-prepared Dox-loaded hpDNA-modified $NaYF_4$@SiO_2–Au nanoconjugates. a) Bright-field optical image (left panel) and fluorescence image (right panel) of HeLa cells incubated with Dox-loaded nanoconjugates (500 μg mL^{-1}) for 2 h before and after the irradiation of a 980 nm laser with the exposure time of 10 min. b) Emission intensity profile shows the corresponding fluorescence intensity analyzed from the white line (marked by 1 and 2) on the fluorescence images in (a). c) Cell viability estimated by CellTiter-Blue cell assay after incubation with Dox-loaded nanoconjugates of different particle concentrations (100–1000 μg mL^{-1}) at 37 °C for 24 h with the laser irradiation at 980 nm (Therapy group). Three control groups were also carried out: only laser irradiation (Only laser), without laser irradiation and treatment of Dox-loaded nanoconjugates (Without laser), and with the treatment of DNA-modified nanoconjugates and laser irradiation but without Dox loading (Without Dox). d,e) Flow cytometry analysis and corresponding statistical results of the cell staining with calcein-AM and propidium iodide (PI) after different treatments. * $p < 0.05$. Note that no marked difference was observed between three control groups.

not observe any precipitates in the absence of the linker DNA strand. The melting temperature of the aggregates was determined to be around 55 °C, which is in good agreement with that measured for typical Au nanoparticle–oligonucleotide sandwich structures.[11b]

To demonstrate light-controlled drug release, we loaded doxorubicin (Dox) molecules onto hpDNA-modified $NaYF_4$@SiO_2–Au nanoparticles through sequence-selective binding (Figures S10 and S11, Supporting Information). As shown in Figure 2f, upon irradiation of the nanoconjugates at 980 nm, we observed an intense broadband emission centered at 575 nm, indicating the efficient release of Dox molecules from the nanoconjugates. The drug release is most likely due to the photothermal effect that induces highly localized heating (Figure S12, Supporting Information). Time-dependent photoluminescence investigations manifested that the amount of Dox molecules in the colloidal solution increased substantially over a short period of time (Figure 2g). By comparison, without laser exposure, the emission intensity of the colloidal solution at 575 nm was kept essentially constant, suggesting the existence of strong bonding between Dox and hpDNA molecules at room temperature. This strong bonding interaction can minimize the potential leakage of drug molecules from the nanoparticulate carrier during the cellular uptake process. As a result, fewer molecules of the therapeutic agent are needed for loading, which would lessen the chance of undesirable side effects.

Prior to investigation of intracellular drug release, we determined the cytotoxicity of the as-prepared nanoconjugates to HeLa cells using CellTiter-Blue cell assay. It was found that the Dox-loaded nanoconjugates virtually did not influence cell growth within 24 h at a concentration range of 100–1000 μg mL^{-1}. In all cases tested, the cell viabilities are greater than 90% (Figure S13, Supporting Information). Subsequently, the event of drug release occurring inside the HeLa cells was monitored using a confocal microscope equipped with a xenon lamp. As shown in **Figure 3**a, without the laser irradiation at 980 nm, only a weak emission of Dox molecules is detectable, which can be attributed to the fluorescence quenching by Au nanoparticles. In stark contrast, with the laser irradiation at 980 nm, we observed an enhanced Dox fluorescence, implying the release of Dox molecules from the particle's surface. The mean fluorescence intensity of the cells treated with laser

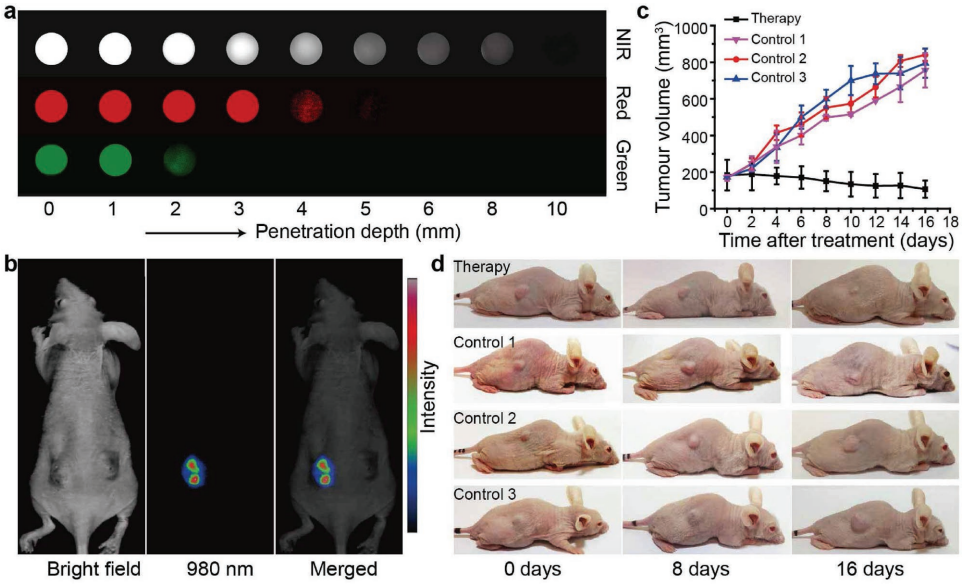

Figure 4. Deep tissue imaging and in vivo photothermal therapy of a subcutaneous tumor injected with Dox-loaded hpDNA-modified $NaYF_4$@SiO_2–Au nanoconjugates. a) CCD imaging of NIR (800 nm), red (660 nm), and green (540 nm) emissions, recorded for the as-prepared $NaYF_4$@SiO_2–Au nanoconjugates and $NaYF_4$:Yb/Er(18:2 mol%)@$NaYF_4$ nanocrystals, under pork muscle tissues of different depth. False-color images were taken under the 980 nm laser excitation. Note that the intensities of the two particle systems at the tissue surface are almost the same. b) In vivo upconversion imaging of the tumor-bearing mouse treated with the DNA-modified nanoconjugates. c) Volumetric changes of the HeLa tumor, compiled as a function of duration time in four different modes of treatment. The tumor volume was normalized to their initial sizes. For the Therapy group, six tumor-bearing mice were injected with Dox-loaded nanoconjugates at the tumor site and then irradiated with a 980 nm laser (500 mW cm^{-2} for 5 min). Three groups of mice were used as controls: only laser irradiation (Control 1), without laser irradiation and treatment of nanoconjugates (Control 2), and with treatment of Dox-loaded nanoconjugates but without laser irradiation (Control 3). d) The corresponding photographs of the tumor-bearing mice taken after various treatments.

irradiation is 2.3-fold higher than that of the cells without the treatment of laser irradiation (Figure 3b and Figure S14 (Supporting Information)). The z-stacks of cell images reveal that the Dox molecules were released and randomly distributed inside the cells (Figure S15, Supporting Information).

We further carried out cell viability assay to evaluate the therapeutic outcome after drug release. As shown in Figure 3c, after the exposure of a 980 nm laser, the cell viability dramatically decreased upon increasing the concentration of Dox-loaded nanoconjugates. In stark contrast, without the laser exposure, the viability level of the HeLa cells after incubation with Dox-loaded nanoconjugates did not show an obvious sign of decrease. In addition, we found that two other control experiments, carried out only under laser exposure or with the combined use of DNA-modified nanoconjugates and laser irradiation, resulted in no appreciable cytotoxicity (Figure 3c). To further study the effect of drug release on the HeLa cells, we conducted flow cytometry analysis to quantitatively evaluate the cell viability. In our experiment, calcein-AM and propidium iodide staining techniques were used to determine the viable and dead cells, respectively. As a result, we found that the cell viability significantly decreases to 1.5% for the Therapy groups, while no obvious cell death is detectable for three control groups (Figure 3d,e). The therapeutic effect was further confirmed by fluorescence imaging (Figure S16, Supporting Information). Taken together, these data suggest that the light-controlled drug release leads to an effective therapeutic outcome. To examine the cellular uptake of the nanoconjugates, we incubated Dox-loaded nanoconjugates with HeLa cells and subsequently carried out cryo-TEM characterization of the tissue specimen. As anticipated, we observed that the nanoconjugates were located within the cellular vesicles (Figure S17, Supporting Information), indicating a successful internalization by the HeLa cells.

The as-prepared $NaYF_4$@SiO_2–Au nanoconjugates feature both excitation and emission bands inside the NIR window, rendering low tissue autofluorescence and thus negligible background signals. Additionally, the NIR emission further offers a depth of penetration much deeper than that achievable by shorter wavelength visible emission. As such, these NIR-to-NIR upconversion nanoconjugates are ideal for ex vivo or in vivo bioimaging and labeling applications. As a proof-of-concept experiment, we placed an agarose gel containing the nanoconjugates and the controls ($NaYF_4$:Yb/Er@$NaYF_4$ nanocrystals) underneath a series of pork tissues of different thickness and imaged them by a home-made in vivo imaging system. As shown in **Figure 4**a, the penetration depths of the green emission around 540 nm and the red emission around 660 nm were determined to be at about 2 and 5 mm, respectively. By comparison, the NIR emission at 800 nm from the nanoconjugates was able to penetrate through 8 mm thick pork tissue. Next, we further evaluate the efficacy of the nanoconjugates as in vivo luminescent probes in imaging tumor-bearing mice. In our design, we used a nude mouse (Balb/c) with two tumors grown at both thighs. A buffer solution of the as-prepared nanoconjugates was then directly injected into the tumor site locating at the left thigh (≈6 mm). As shown in Figure 4b, the upconverted NIR emission can be detected from the injection site.

We further examined the therapeutic effects of the as-synthesized nanoconjugates upon drug release in the tumor-bearing mice. In a typical experiment, we intratumorally injected Dox-loaded nanoconjugates into the tumor site followed by 980 nm laser irradiation. The tumor size was measured every 2 d after treatment. We found that the size of the tumor after exposure to NIR laser gradually decreased, indicating a successful drug release into the tumor site (Figure 4c,d). By comparison, all three control experiments (Control 1: only laser irradiation; Control 2: without laser irradiation and treatment of nanoconjugates; Control 3: with treatment of Dox-loaded nanoconjugates but without laser irradiation) showed a marked increase in the tumor size. The histologic images of hematoxylin and eosin-stained tumor slices showed that a large area of dead cells without nuclei in the tumor tissue after photothermal drug release could be clearly observed. These results confirm that the therapeutic effect originates from the drug molecules released from the injected nanoconjugates. Meanwhile, no obvious pathological abnormalities in various organs such as liver, kidney, and spleen could be found, manifesting the excellent biocompatibility of the as-prepared nanoconjugates (Figure S18, Supporting Information).

In summary, we have developed an imaging-guided upconversion nanothermometry approach for deep-tissue drug delivery. The design and fabrication of hpDNA-functionalized $NaYF_4$@SiO_2–Au nanoconjugates has enabled the demonstration of excitation and emission processes both in the first biological window, which makes these nanoconjugates as promising probes for deep-tissue imaging and guided therapy. In addition, the hpDNA molecules tethered on the particle's surface largely improved the dispersibility of the nanoparticles in physiological environment. Significantly, the hpDNA endowed the as-prepared nanoconjugates surface with dual functions. Beyond the benefit of serving as an effective carrier for many DNA-binding drug molecules, the hpDNA also allows the process of drug release to be precisely controlled by the photothermal effect owing to its high sensitivity to fluctuations in temperature. Our in vitro and in vivo studies establish a new modality ideally suited for simultaneous deep-tissue imaging and drug molecule release.

Experimental Section

The experimental details are provided in the Supporting Information.

Supporting Information

Supporting Information is available from the Wiley Online Library or from the author.

Acknowledgements

This work was supported by the Singapore Ministry of Education (Grant R143000627112, R143000642112), the Singapore Institute for Neurotechnology (R175000121733), the NUHS Clinician Research Grant (R175000133733), the National Research Foundation, Prime Minister's Office, Singapore under its Competitive Research Program (CRP Award No. NRF-CRP15-2015-03), the National Basic Research Program of China (973 Program, Grant 2015CB932200), the National Natural Science Foundation of China (61136003), the Natural Science Foundation of Jiangsu Province (BE2015699), and the CAS/SAFEA International Partnership Program for Creative Research Teams. The authors thank Dr. Paul Hutchinson for technical support on flow cytometry. The authors thank J.T., Q.S., X.Q., and X.L. for helpful discussions. All procedures for animal experiments were approved by the Institutional Animal Care and Use Committee (IACUC # 151036) at the Agency for Science, Technology and Research (A*STAR) of Singapore.

Received: January 12, 2017
Published online: March 10, 2017

[1] a) M. Bruchez Jr., M. Moronne, P. Gin, S. Weiss, A. P. Alivisatos, *Science* **1998**, *281*, 2013; b) X. Gao, Y. Cui, R. M. Levenson, L. W. K. Chung, S. Nie, *Nat. Biotechnol.* **2004**, *22*, 969; c) Y. Il Park, K. T. Lee, Y. D. Suh, T. Hyeon, *Chem. Soc. Rev.* **2015**, *44*, 1302; d) X. Zhang, F. Ai, T. Sun, F. Wang, G. Zhu, *Inorg. Chem.* **2016**, *55*, 3872; e) J. Zhou, Z. Liu, F. Li, *Chem. Soc. Rev.* **2012**, *41*, 1323; f) Q. Ju, X. Chen, F. Ai, D. Peng, X. Lin, W. Kong, P. Shi, G. Zhu, F. Wang, *J. Mater. Chem. B* **2015**, *3*, 3548; g) C. Ma, T. Bian, S. Yang, C. Liu, T. Zhang, J. Yang, Y. Li, J. Li, R. Yang, W. Tan, *Anal. Chem.* **2014**, *86*, 6508; h) S. Han, R. Deng, X. Xie, X. Liu, J. Zhou, *Angew. Chem. Int. Ed.* **2014**, *53*, 11702; i) Z. Yi, X. Li, Z. Xue, X. Liang, W. Lu, H. Peng, H. Liu, S. Zeng, J. Hao, *Adv. Funct. Mater.* **2015**, *25*, 7119.

[2] a) C. W. T. Leung, Y. Hong, S. Chen, E. Zhao, J. W. Y. Lam, B. Z. Tang, *J. Am. Chem. Soc.* **2013**, *135*, 62; b) I. L. Medintz, H. T. Uyeda, E. R. Goldman, H. Mattoussi, *Nat. Mater.* **2005**, *4*, 435; c) P. Huang, W. Zheng, S. Zhou, D. Tu, Z. Chen, H. Zhu, R. Li, E. Ma, M. Huang, X. Chen, *Angew. Chem., Int. Ed.* **2014**, *53*, 1252; d) J. Zhou, Q. Liu, W. Feng, Y. Sun, F. Li, *Chem. Rev.* **2015**, *115*, 395; e) W. Zheng, P. Huang, D. Tu, E. Ma, H. Zhu, X. Chen, *Chem. Soc. Rev.* **2015**, *44*, 1379; f) L. Sun, Y. Wang, C. Yan, *Acc. Chem. Res.* **2014**, *47*, 1001; g) M.-K. Tsang, W. Ye, G. Wang, J. Li, M. Yang, J. Hao, *ACS Nano* **2016**, *10*, 598.

[3] a) D. R. Larson, W. R. Zipfel, R. M. Williams, S. W. Clark, M. P. Bruchez, F. W. Wise, W. W. Webb, *Science* **2003**, *300*, 1434; b) G. Lukinavičius, L. Reymond, E. D'Este, A. Masharina, F. Göttfert, H. Ta, A. Güther, M. Fournier, S. Rizzo, H. Waldmann, C. Blaukopf, C. Sommer, D. W Gerlich, H.-D. Arndt, S. W Hell, K. Johnsson, *Nat. Methods* **2014**, *11*, 731; c) H. S. Park, S. H. Nam, J. Kim, H. S. Shin, Y. D. Suh, K. S. Hong, *Sci. Rep.* **2016**, *6*, 27407; d) S. Shah, J.-J. Liu, N. Pasquale, J. Lai, H. McGowan, Z. P. Pang, K.-B. Lee, *Nanoscale* **2015**, *7*, 16571; e) D. Ni, J. Zhang, W. Bu, H. Xing, F. Han, Q. Xiao, Z. Yao, F. Chen, Q. He, J. Liu, S. Zhang, W. Fan, L. Zhou, W. Peng, J. Shi, *ACS Nano* **2014**, *8*, 1231.

[4] a) M. A. Whitney, J. L. Crisp, L. T. Nguyen, B. Friedman, L. A. Gross, P. Steinbach, R. Y Tsien, Q. T. Nguyen, *Nat. Biotechnol.* **2011**, *29*, 352; b) Y. Urano, D. Asanuma, Y. Hama, Y. Koyama, T. Barrett, M. Kamiya, T. Nagano, T. Watanabe, A. Hasegawa, P. L. Choyke, H. Kobayashi, *Nat. Med.* **2008**, *15*, 104; c) L. Cheng, C. Wang, L. Feng, K. Yang, Z. Liu, *Chem. Rev.* **2014**, *114*, 10869; d) M. Wang, Z. Chen, W. Zheng, H. Zhu, S. Lu, E. Ma, D. Tu, S. Zhou, M. Huang, X. Chen, *Nanoscale* **2014**, *6*, 8274.

[5] a) A. L. Antaris, H. Chen, K. Cheng, Y. Sun, G. Hong, C. Qu, S. Diao, Z. Deng, X. Hu, B. Zhang, X. Zhang, O. K. Yaghi, Z. R. Alamparambil, X. Hong, Z. Cheng, H. Dai, *Nat. Mater.* **2016**, *15*, 235; b) G. Chen, T. Y. Ohulchanskyy, R. Kumar, H. Agren, P. N. Prasad, *ACS Nano* **2010**, *4*, 3163; c) J.-C. G. Bünzli, *Chem. Rev.* **2010**, *110*, 2729; d) F. Auzel, *Chem. Rev.* **2004**, *104*, 139; e) M. Bettinelli, L. Carlos, X. Liu, *Phys. Today* **2015**, *68*, 38;

f) G. Chen, H. Qiu, P. N. Prasad, X. Chen, *Chem. Rev.* **2014**, *114*, 5161; g) C. Yao, P. Wang, R. Wang, L. Zhou, A. M. El-Toni, Y. Lu, X. Li, F. Zhang, *Anal. Chem.* **2016**, *137*, 2808.

[6] a) B. Zhou, B. Shi, D. Jin, X. Liu, *Nat. Nanotechnol.* **2015**, *10*, 924; b) M. Haase, H. Schäfer, *Angew. Chem., Int. Ed.* **2011**, *50*, 5808; c) A. Speghini, F. Piccinelli, M. Bettinelli, *Opt. Mater.* **2011**, *33*, 247; d) L. Zhou, R. Wang, C. Yao, X. Li, C. Wang, X. Zhang, C. Xu, A. Zeng, D. Zhao, F. Zhang, *Nat. Commun.* **2015**, *6*, 6938; e) J. Zhao, D. Jin, E. P. Schartner, Y. Lu, Y. Liu, A. V. Zvyagin, L. Zhang, J. M. Dawes, P. Xi, J. A. Piper, E. M. Goldys, T. M. Monro, *Nat. Nanotechnol.* **2013**, *8*, 729; f) S. Han, X. Qin, Z. An, Y. Zhu, L. Liang, Y. Han, W. Huang, X. Liu, *Nat. Commun.* **2016**, *7*, 13059; g) M.-K. Tsang, G. Bai, J. Hao, *Chem. Soc. Rev.* **2015**, *44*, 1585; h) P. Rodríguez-Sevilla, Y. Zhang, P. Haro-González, F. Sanz-Rodríguez, F. Jaque, J. G. Solé, X. Liu, D. Jaque, *Adv. Mater.* **2016**, *28*, 2421; i) C. D. S. Brites, X. Xie, M. L. Debasu, X. Qin, R. Chen, W. Huang, J. Rocha, X. Liu, L. D. Carlos, *Nat. Nanotechnol.* **2016**, *11*, 851; j) Y. Yang, Q. Shao, R. Deng, C. Wang, X. Teng, K. Cheng, Z. Cheng, L. Huang, Z. Liu, X. Liu, B. Xing, *Angew. Chem., Int. Ed.* **2012**, *51*, 3125; k) X. Chen, L. Jin, W. Kong, T. Sun, W. Zhang, X. Liu, J. Fan, S. F. Yu, F. Wang, *Nat. Commun.* **2016**, *7*, 10304; l) H. Schäfer, P. Ptacek, H. Eickmeier, M. Haase, *Adv. Funct. Mater.* **2009**, *19*, 3091; m) X. Li, F. Zhang, D. Zhao, *Chem. Soc. Rev.* **2015**, *44*, 1346.

[7] a) X. Wu, Y. Zhang, K. Takle, O. Bilsel, Z. Li, H. Lee, Z. Zhang, D. Li, W. Fan, C. Duan, E. M. Chan, C. Lois, Y. Xiang, G. Han, *ACS Nano* **2016**, *10*, 1060; b) E. M. Chan, *Chem. Soc. Rev.* **2015**, *44*, 1653; c) J. Lai, B. P. Shah, Y. Zhang, L. Yang, K.-B. Lee, *ACS Nano* **2015**, *9*, 5234; d) L. Cheng, K. Yang, Y. Li, J. Chen, C. Wang, M. Shao, S.-T. Lee, Z. Liu, *Angew. Chem., Int. Ed.* **2011**, *50*, 7385; e) J. Liu, W. Bu, J. Shi, *Acc. Chem. Res.* **2015**, *48*, 1797; f) X. Liu, I. Que, X. Kong, Y. Zhang, L. Tu, Y. Chang, T. Wang, A. Chan, C. W. G. M. Löwik, H. Zhang, *Nanoscale* **2015**, *7*, 14914; g) A. Punjabi, X. Wu, A. Tokatli-Apollon, M. El-Rifai, H. Lee, Y. Zhang, C. Wang, Z. Liu, E. M. Chan, C. Duan, G. Han, *ACS Nano* **2014**, *8*, 10621; h) N. M. Idris, M. K. Gnanasammandhan, J. Zhang, P. C. Ho, R. Mahendran, Y. Zhang, *Nat. Med.* **2012**, *18*, 1580; i) Y. Wang, G. Liu, L. Sun, J. Xiao, J. Zhou, C. Yan, *ACS Nano* **2013**, *7*, 7200; j) W. Li, J. Wang, J. Ren, X. Qu, *J. Am. Chem. Soc.* **2014**, *136*, 2248; k) X. Zhu, W. Feng, J. Chang, Y. Tan, J. Li, M. Chen, Y. Sun, F. Li, *Nat. Commun.* **2016**, *7*, 10437; l) Y. Dai, H. Xiao, J. Liu, Q. Yuan, P. Ma, D. Yang, C. Li, Z. Cheng, Z. Hou, P. Yang, J. Lin, *J. Am. Chem. Soc.* **2013**, *135*, 18920; m) X. Z. Ai, C. J. H. Ho, J. Aw, A. B. E. Attia, J. Mu, Y. Wang, X. Wang, Y. Wang, X. Liu, H. Chen, M. Gao, X. Chen, E. K. L. Yeow, G. Liu, M. Olivo, B. Xing, *Nat. Commun.* **2016**, *7*, 10432; n) Y. Yang, F. Liu, X. Liu, B. Xing, *Nanoscale* **2013**, *5*, 231.

[8] a) S. Wu, G. Han, D. J. Milliron, S. Aloni, V. Altoe, D. V. Talapin, B. E. Cohen, P. J. Schuck, *Proc. Natl. Acad. Sci. USA* **2009**, *106*, 10917; b) N. Bogdan, F. Vetrone, R. Roy, J. A. Capobianco, *J. Mater. Chem.* **2010**, *20*, 7543; c) S. H. Nam, Y. M. Bae, Y. Il Park, J. H. Kim, H. M. Kim, J. S. Choi, K. T. Lee, T. Hyeon, Y. D. Suh, *Angew. Chem., Int. Ed.* **2011**, *50*, 6093; d) T. V. Esipova, X. Ye, J. E. Collins, S. Sakadžić, E. T. Mandeville, C. B. Murray, S. A. Vinogradov, *Proc. Natl. Acad. Sci. USA* **2012**, *109*, 20826; e) G. Tian, Z. Gu, L. Zhou, W. Yin, X. Liu, L. Yan, S. Jin, W. Ren, G. Xing, S. Li, Y. Zhao, *Adv. Mater.* **2012**, *24*, 1226; f) P. Ma, H. Xiao, X. Li, C. Li, Y. Dai, Z. Cheng, X. Jing, J. Lin, *Adv. Mater.* **2013**, *25*, 4898; g) L. Li, R. Zhang, L. Yin, K. Zheng, W. Qin, P. R. Selvin, Y. Lu, *Angew. Chem., Int. Ed.* **2012**, *51*, 6121.

[9] a) H. Dong, S. Du, X. Zheng, G. Lyu, L. Sun, L. Li, P. Zhang, C. Zhang, C. Yan, *Chem. Rev.* **2015**, *115*, 10725; b) J. Lu, Y. Chen, D. Liu, W. Ren, Y. Lu, Y. Shi, J. Piper, I. Paulsen, D. Jin, *Anal. Chem.* **2015**, *87*, 10406; c) S. Gai, C. Li, P. Yang, J. Lin, *Chem. Rev.* **2014**, *114*, 2343; d) Y. Liu, D. Tu, H. Zhu, X. Chen, *Chem. Soc. Rev.* **2013**, *42*, 6924; e) Q. Yuan, Y. Wu, J. Wang, D. Lu, Z. Zhao, T. Liu, X. Zhang, W. Tan, *Angew. Chem., Int. Ed.* **2013**, *52*, 13965; f) Y. Cen, Y. Wu, X. Kong, S. Wu, R. Yu, X. Chu, *Anal. Chem.* **2014**, *86*, 7119.

[10] a) C. Drees, A. N. Raj, R. Kurre, K. B. Busch, M. Haase, J. Piehler, *Angew. Chem., Int. Ed.* **2016**, *55*, 11668; b) L. Wang, R. Yan, Z. Huo, L. Wang, J. Zeng, J. Bao, X. Wang, Q. Peng, Y. Li, *Angew. Chem., Int. Ed.* **2005**, *44*, 6054; c) H. S. Mader, P. Kele, S. M. Saleh, O. S. Wofbeis, *Curr. Opin. Chem. Biol.* **2010**, *14*, 582; d) F. Meiser, C. Cortez, F. Caruso, *Angew. Chem., Int. Ed.* **2004**, *43*, 5954.

[11] a) C. Zhang, R. J. Macfarlane, K. L. Young, C. H. J. Choi, L. Hao, E. Auyeung, G. Liu, X. Zhou, C. A. Mirkin, *Nat. Mater.* **2013**, *12*, 741; b) X. Xue, F. Wang, X. Liu, *J. Am. Chem. Soc.* **2008**, *130*, 3244; c) Y. Cao, R. Jin, C. A. Mirkin, *J. Am. Chem. Soc.* **2001**, *123*, 7961; d) Z. Wu, G. Liu, X. Yang, J. Jiang, *J. Am. Chem. Soc.* **2015**, *137*, 6829.

[12] a) Y.-L. Luo, Y.-S. Shiao, Y.-F. Huang, *ACS Nano* **2011**, *5*, 7796; b) Y. Wang, C. Zhang, L. Tang, J. Jiang, *Anal. Chem.* **2012**, *84*, 8602; c) M. R. Jones, N. C. Seeman, C. A. Mirkin, *Science* **2015**, *347*, 1260901; d) L. Li, Y. Lu, *J. Am. Chem. Soc.* **2015**, *137*, 5272.

[13] a) J. C. Boyer, M. P. Manseau, J. I. Murray, F. C. van Veggel, *Langmuir* **2010**, *26*, 1157; b) L. Li, P. Wu, K. Hwang, Y. Lu, *J. Am. Chem. Soc.* **2013**, *135*, 2411; c) J. Li, C. Hong, S. Wu, H. Liang, L. Wang, G. Huang, X. Chen, H. Yang, D. Shangguan, W. Tan, *J. Am. Chem. Soc.* **2015**, *137*, 11210; d) L. Huang, R. Yu, X. Chu, *Analyst* **2015**, *140*, 4987; e) Z. Chen, H. Chen, H. Hu, M. Yu, F. Li, Q. Zhang, Z. Zhou, T. Yi, C. Huang, *J. Am. Chem. Soc.* **2008**, *130*, 3023; f) R. Li, Z. Ji, J. Dong, C. H. Chang, X. Wang, B. Sun, M. Wang, Y.-P. Liao, J. I. Zink, A. E. Nel, T. Xia, *ACS Nano* **2015**, *9*, 3293; g) J. Tian, X. Zeng, X. Xie, S. Han, O.-W. Liew, Y.-T. Chen, L. Wang, X. Liu, *J. Am. Chem. Soc.* **2015**, *137*, 6550; h) C. Yao, C. Wei, Z. Huang, Y. Lu, A. M. El-Toni, D. Ju, X. Zhang, W. Wang, F. Zhang, *ACS Appl. Mater. Interfaces* **2016**, *8*, 6935.

[14] T. Junt, W. Barchet, *Nat. Rev. Immunol.* **2015**, *15*, 529.

[15] a) F. Wang, Y. Han, C. S. Lim, Y. Lu, J. Wang, J. Xu, H. Chen, C. Zhang, M Hong, X. Liu, *Nature* **2010**, *463*, 1061; b) F. Wang, R. Deng, X. Liu, *Nat. Protoc.* **2014**, *9*, 1634.

[16] W. Stöber, A. Fink, *J. Colloid Interface Sci.* **1968**, *26*, 62.

[17] a) M. P. Singh, G. F. Strouse, *J. Am. Chem. Soc.* **2010**, *132*, 9383; b) G. P. Wiederrecht, G. A. Wurtz, J. Hranisavljevic, *Nano Lett.* **2004**, *4*, 2121.